catalysts

MDPI

Article

Nickel Supported on $AlCeO_3$ as a Highly Selective and Stable Catalyst for Hydrogen Production via the Glycerol Steam Reforming Reaction

Nikolaos D. Charisiou [1], Georgios I. Siakavelas [1], Binlin Dou [2], Victor Sebastian [3,4], Steven J. Hinder [5], Mark A. Baker [5], Kyriaki Polychronopoulou [6,7,*] and Maria A. Goula [1,*]

1 Department of Environmental and Pollution Control Engineering, Laboratory of Alternative Fuels and Environmental Catalysis (LAFEC), Western Macedonia University of Applied Sciences, GR-50100 Kila, Greece; ncharis@teiwm.gr (N.D.C.); giorgosiakavelas@gmail.com (G.I.S.)
2 School of Energy and Power Engineering, University of Shanghai for Science and Technology, Shanghai 200093, China; bldou@usst.edu.cn
3 Chemical and Environmental Engineering Department, Instituto de Nanociencia de Aragón (INA) and Instituto de Ciencia de Materiales de Aragón (ICMA), Universidad de Zaragoza-CSIC, 50018 Zaragoza, Spain; victorse@unizar.es
4 Networking Research Center on Bioengineering, Biomaterials and Nanomedicine, CIBERBBN, 28029 Madrid, Spain
5 The Surface Analysis Laboratory, Faculty of Engineering and Physical Sciences, University of Surrey, Guildford GU2 4DL, UK; s.hinder@surrey.ac.uk (S.J.H.); m.baker@surrey.ac.uk (M.A.B.)
6 Department of Mechanical Engineering, Khalifa University of Science and Technology, Abu Dhabi P.O. Box 127788, UAE
7 Center for Catalysis and Separation, Khalifa University of Science and Technology, Abu Dhabi P.O. Box 127788, UAE
* Correspondence: kyriaki.polychrono@ku.ac.ae (K.P.); mgoula@teiwm.gr (M.A.G.); Tel.: +971-2-401-8211 (K.P.); +30-24610-68296 (M.A.G.)

Received: 8 April 2019; Accepted: 19 April 2019; Published: 1 May 2019

check for updates

Abstract: In this study, a critical comparison between two low metal (Ni) loading catalysts is presented, namely Ni/Al_2O_3 and $Ni/AlCeO_3$ for the glycerol steam reforming (GSR) reaction. The surface and bulk properties of the catalysts were evaluated using a plethora of techniques, such as N_2 adsorption/desorption, Inductively Coupled Plasma Atomic Emission Spectroscopy (ICP–AES), X-ray Diffraction (XRD), X-ray Photoelectron Spectroscopy (XPS), Scanning Electron Microscopy / Energy Dispersive X-Ray Spectroscopy (SEM/EDX, Transmission Electron Microscopy (TEM), CO_2 and NH_3–Temperature Programmed Desorption (TPD), and Temperature Programmed Reduction (H_2–TPR). Carbon deposited on the catalyst's surfaces was probed using Temperature Programmed Oxidation (TPO), SEM, and TEM. It is demonstrated that Ce-modification of Al_2O_3 induces an increase of the surface basicity and Ni dispersion. These features lead to a higher conversion of glycerol to gaseous products (60% to 80%), particularly H_2 and CO_2, enhancement of WGS reaction, and a higher resistance to coke deposition. Allyl alcohol was found to be the main liquid product for the $Ni/AlCeO_3$ catalyst, the production of which ceases over 700 °C. It is also highly significant that the $Ni/AlCeO_3$ catalyst demonstrated stable values for H_2 yield (2.9–2.3) and selectivity (89–81%), in addition to CO_2 (75–67%) and CO (23–29%) selectivity during a (20 h) long time-on-stream study. Following the reaction, SEM/EDX and TEM analysis showed heavy coke deposition over the Ni/Al_2O_3 catalyst, whereas for the $Ni/AlCeO_3$ catalyst TPO studies showed the formation of more defective coke, the latter being more easily oxidized.

Keywords: nickel catalysts; ceria; alumina; glycerol steam reforming; H_2 production

1. Introduction

Biofuels are expected to play an important role in meeting the combined challenge of providing adequate energy supplies, while simultaneously combating the threat posed by climate change, with projections estimating that their use will grow from 1.3 million barrels of oil equivalent (BOE) in 2012 to 4.6 BOE in 2040 [1]. Although biodiesel had captured approximately 25% of total biofuel output in 2015 [2], the high costs associated with its production means that the sector remains uncompetitive, with favourable government policies underpinning much of its growth [3]. The industry is also facing the challenge of dealing, in a sustainable way, with the co-production of crude glycerol ($C_3H_8O_3$), which constitutes its major by-product and amounts to approximately 10 wt % of the oil undergoing transesterification [4].

However, glycerol can be converted into hydrogen, a fuel that finds a variety of present-day applications in transport, building and other industry sectors, while at the same time is expected to have a leading role in a future carbon-free energy mix [5]. Although different thermochemical processes may be used for the conversion of $C_3H_8O_3$ into H_2—e.g., aqueous phase reforming (APR), autothermal reforming (ATR) and super critical water reforming (SCWR)—the process that appears most promising is that of the steam reforming of glycerol (GSR) [6–8]. This is because GSR has a high H_2 production capacity per mol of $C_3H_8O_3$ reformed (Equation (1)) and is a mature industrial technology unlikely to require major technical adjustments in switching feedstocks [9,10]. The GSR (Equation (1)), a strongly endothermic reaction (ΔH^{Θ} = 123 kJ/mole), combines the decomposition of glycerol (Equation (2)) and the water-gas shift reaction (WGS, Equation (3)), but a number of parallel reactions that include methanation (Equation (4)), methane dry reforming (Equation (5)) and carbon formation reactions (Equations (6)–(9)) also take place [11,12]. According to the thermodynamic studies undertaken, the GSR should be undertaken at high temperature (>630 °C), high water to glycerol feed ratio (WGFR < 9:1, molar) and at atmospheric pressure [13,14].

$$C_3H_8O_3 + 3H_2O \rightarrow 3CO_2 + 7H_2, \quad (1)$$

$$C_3H_8O_3 \rightarrow 3CO + 4H_2, \quad (2)$$

$$CO + H_2O \leftrightarrow CO_2 + H_2, \quad (3)$$

$$CO + 3H_2 \leftrightarrow CH_4 + H_2O, \quad (4)$$

$$CH_4 + CO_2 \leftrightarrow 2H_2 + 2CO, \quad (5)$$

$$2CO \leftrightarrow CO_2 + C, \quad (6)$$

$$CH_4 \leftrightarrow 2H_2 + C, \quad (7)$$

$$H_2O + C \leftrightarrow CO + H_2, \quad (8)$$

$$C_3H_8O_3 \rightarrow H_2 + 3H_2O + 3C, \quad (9)$$

To be effective, the catalysts for use in the GSR should not promote C–O cleavage and CO or CO_2 hydrogenation, but they should favour the cleavage of the C–H, C–C and O–H bonds [15,16]. As Ni-based systems are known to be highly active in reforming reactions, most efforts currently found in the GSR related literature have focused on the development of such catalysts, using a variety of metal oxides (e.g., Al_2O_3, ZrO_2, SiO_2) as supports [17–20]. The most commonly used support is Al_2O_3 as it possesses a number of desirable properties, such as chemical and mechanical resistance under reaction conditions and a high specific surface area, which favours the dispersion of the active phase on the support [20,21]. However, there are two main disadvantages associated with the use of alumina; firstly, the Lewis type acid sites that it possesses promote acid-base-catalyzed reactions, which in turn favour the formation of a filamentous type of carbon, and secondly, it fosters the sintering of metallic particles [22,23]. For example, Chiodo et al. [24], using a low steam to glycerol ratio (3 mol/mol) and testing the stability at 800 °C for 20 h, reported rapid deactivation for a Ni/Al catalyst (30 wt % Ni). Cheng et al. [25], reported significant carbon deposition for a Ni/Al (15 wt % Ni) at 550 °C tested for approximately 4 h, even under excess steam conditions. Previous work by our group [15] showed severe deactivation for a Ni/Al (8 wt % Ni) during 20 h time-on-stream at 600 °C (WGFR of 9/1, molar), which was attributed to the high degree of crystallinity of the carbon deposits. Thus, much effort has been spent on overcoming the disadvantages associated with the use of alumina by inducing support-mediated promotional effects using different alkaline earth metals (e.g., Mg, Ca), lanthanide metals (e.g., Ce, La), and/or transition metals (e.g., Zr, Cu) as promoters for Ni/Al catalysts [26–28].

As is well understood, ceria can affect the surface acidity of alumina due to its higher point of zero charge (PZC) [29]. It also has the ability to act as an O_2 buffer, storing/releasing O_2 via the Ce^{3+}/Ce^{4+} redox couple in CeO_2 [30], and thus promote water dissociation and the water gas shift reaction [31]. Recent research also suggests that a [$O^{\delta-}$, δ^+] dipolar layer is created on the surface of Ni particles that can protect them against thermal sintering [32–34]. For the GSR, a handful of works exist where ceria was used as promoter to alumina for Ni-based catalysts [35–38]. The general conclusion from these papers is that the addition of CeO_2 as alumina modifier enhances the activity of the non-promoted catalyst [35–37]. This is mainly related to the ability of ceria to stabilize the nickel particles and to promote steam reforming of the oxygenated hydrocarbons intermediates, leading to a reduction in coke deposition. It has also been suggested that ceria hinders secondary dehydration reactions (favoured by the presence of acid sites in the support), and lead to the formation of hydrocarbons that are coke precursors (and thus, responsible for catalyst deactivation) [38]. It has also been suggested that the formation of a $CeAlO_3$ perovskite structure can suppress the interaction between Ni and Al_2O_3 and increase the number of active Brønsted acid sites. This, in turn, improves the bifunctional metal-acid properties of Ni/CeO_2–Al_2O_3 and favours the hydrogenolysis and dehydrogenation-dehydration of condensable intermediate products that produce more H_2 [39].

In the present investigation, low metal loading (8 wt %) Ni catalysts supported on γ-Al_2O_3 and γ-Al_2O_3 modified with CeO_2 were investigated in terms of catalytic activity and time-on-stream stability during the GSR. Different characterization techniques, i.e., N_2-physisorption, ICP, XRD, temperature programmed reduction (H_2–TPR), CO_2–TPD, NH_3–TPD, XPS, TPO, SEM and TEM were used in an effort to identify the catalyst surface and bulk properties which affect the reaction and its products. The performance of the catalysts was investigated with the aim of identifying the effect of temperature on the total conversion of glycerol and the conversion of glycerol to gaseous products, the selectivity towards H_2, CO_2, CO, CH_4 and the liquid effluents produced during the reaction and for the determination of the H_2/CO and CO/CO_2 molar ratio in the gaseous products mixture. Time-on-stream experiments were conducted for 20 h under harsh reaction conditions in order to induce carbon deposition and the main liquid effluents were quantified.

2. Results and Discussion

2.1. Characterization Results

2.1.1. Chemical Analysis and Textural Properties

The physicochemical, structural and textural properties of the calcined and reduced catalysts are summarized in Table 1. As a first observation, both catalysts have a similar Ni metal loading, which was measured for the calcined samples at 7.14 and 7.69 wt % for Ni/Al_2O_3 and Ni/$AlCeO_3$, respectively. Regarding the properties of the calcined supports used herein, N_2-physisorption measurements showed that Al_2O_3 has a much higher specific surface area (SSA) than $AlCeO_3$ (195 m^2 g^{-1} compared to 48 m^2 g^{-1}) and pore volume (0.65 cm g^{-1} compared to 0.24 cm g^{-1}). Following Ni impregnation and then catalyst calcination, the SSA of the Ni/Al_2O_3 catalyst dropped to 158 m^2 g^{-1} and then further to 136 m^2 g^{-1} after the reduction procedure. For Ni/$AlCeO_3$, this drop was less pronounced after calcination, but somewhat sharper after reduction (43 m^2 g^{-1} after calcination and 26 m^2 g^{-1} after reduction).

Table 1. Physicochemical, structural and textural properties of calcined and reduced catalysts.

Catalyst	Calcined Samples			Reduced Samples			
	Metal Loading (Ni, wt %)	SSA (m^2g^{-1})	Pore Volume (cm^3g^{-1})	SSA (m^2g^{-1})	Pore Volume (cm^3g^{-1})	Av. Pore Width (nm)	Ni^0 Mean Crystallite Size (nm)
Ni/Al_2O_3	7.14	158	0.58	136	0.32	20.1	16.8
$Ni/AlCeO_3$	7.69	43	0.27	26	0.18	23.5	14.2

Also, for both catalysts, the pore volume remained almost unchanged following calcination, but dropped substantially after reduction. However, the doping of Al_2O_3 with CeO_2 resulted in enhanced basicity, as shown from the potentiometric titration curves obtained for the Al_2O_3 and $AlCeO_3$ suspensions, with the PZC values recorded at 6.8 and 8.2, respectively (Figure 1). It is noted that the PZC is defined as the pH value where the basic and acidic sites on the surface are in equilibrium [40].

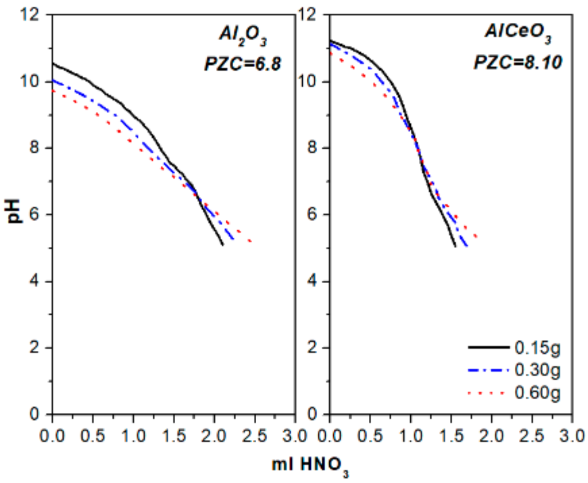

Figure 1. Potentiometric titration curves and point of zero charge (PZC) of the Al_2O_3 and $AlCeO_3$ supports.

The N_2 adsorption—desorption isotherms of both catalysts, displayed as an inset in Figure 2, are of Type IV with an H4-type hysteresis loop [41], and show major adsorption at high pressures (0.7 < P/P0 < 1.0) and only minor adsorption at low pressure ($P/P_0 < 0.05$). This is indicative of mainly mesoporous material with some macroporosity [42] and is corroborated by the corresponding pore size distributions.

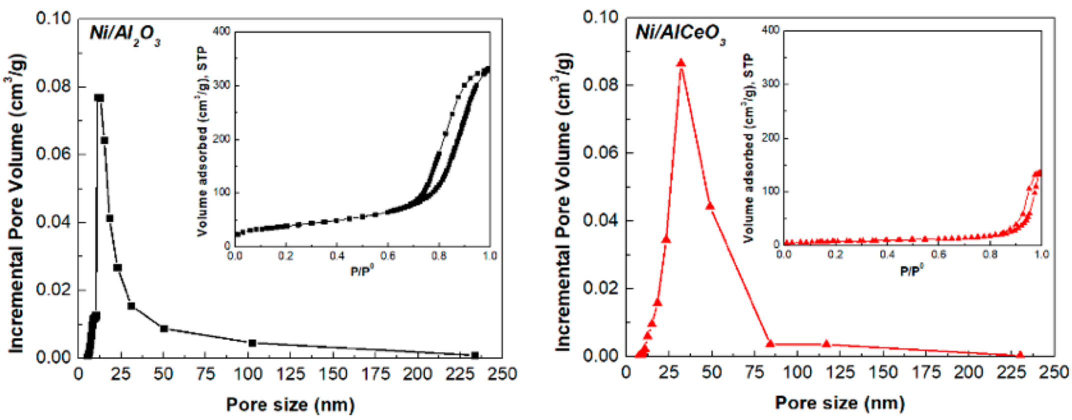

Figure 2. Pore size distribution and N_2 adsorption-desorption isotherms (inset) of the reduced Ni/Al_2O_3 and $Ni/AlCeO_3$ catalysts.

Figure 3 presents the XRD patterns for the supports (after calcination) and catalytic samples (after calcination and after reduction). Regarding the Al_2O_3 support and Ni/Al_2O_3 catalyst, the characteristic peaks of γ-Al_2O_3 are clearly identified at 2θ = 37.2°, 47.2° and 67.2°. The nickel aluminate phase ($NiAl_2O_4$) was observed at 2θ = 19.0°, 32.0°, 37.0°, 45.0°, 60.2° and 65.9° for both calcined and reduced catalysts [43]. However, it is also clear from the diffractograms that the Al_2O_3 and $NiAl_2O_4$ peaks are not as intense on the reduced sample in comparison to the calcined one. Moreover, on the reduced catalyst, two small peaks corresponding to metallic nickel (Ni^0), at 2θ = 44.0° and 51.2° [43], can be observed. For the calcined $AlCeO_3$ support, γ-Al_2O_3 was detected only at 2θ = 67.2° and the crystal phase of CeO_2 dominated with peaks at 2θ = 28.5°, 33.0°, 47.5°, 56.5° and 59.0° (Figure 3b) [44]. The XRD patterns of the Ni/$AlCeO_3$ catalyst after calcination and after reduction (Figure 3b) are nearly identical to the pattern of the calcined $AlCeO_3$ support with the only differences being two small peaks corresponding to $NiAl_2O_4$ detected on the calcined catalyst (2θ = 32.0° and 37.0°), and two peaks, corresponding to Ni^0, detected at 2θ = 43.5° and 50.8° on the reduced sample. It is noted that the reaction $4CeAlO_3 + O_2 \leftrightarrow 4CeO_2 + 2Al_2O_3$ is reversible, i.e., $CeAlO_3$ can be oxidised to CeO_2 by heating in air and CeO_2 can be reduced by heating in H_2 flow [45]. The Ni species mean particle size (Table 1), for the reduced samples, was determined from the XRD spectra using Scherrer analysis and was found at 16.8 nm for the Ni/Al_2O_3 and at 14.2 nm for the Ni/$AlCeO_3$ catalyst.

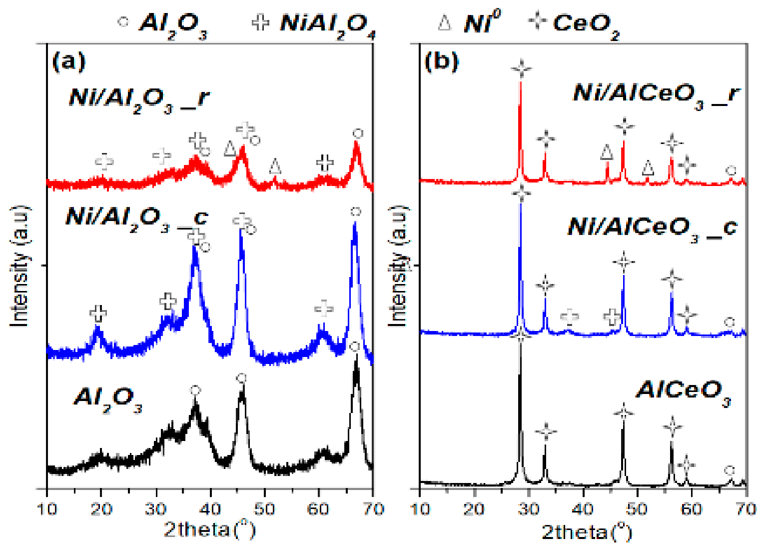

Figure 3. XRD patterns of supports, calcined and reduced catalysts: (**a**) Al_2O_3 and Ni/Al_2O_3 and (**b**) $AlCeO_3$ and Ni/$AlCeO_3$.

2.1.2. Surface Acidity-Basicity Estimation

Figure 4a presents the CO_2–TPD profiles obtained over the Ni/Al_2O_3 and Ni/$AlCeO_3$ catalysts. The Ni/Al_2O_3 catalyst presents mainly two types of basic sites of weak and medium strength. This is reflected by the peaks that appeared in the temperature regimes of 30 °C < T_{max} < 220 °C and 220 °C < T_{max} < 450 °C. The strong basic site population is very limited. On the other hand, it seems that the modification of Al_2O_3 support with Ce leads to a catalyst with a limited population of weak basic sites and a wider distribution of medium strength basic sites, whereas the population of strong basic sites is enhanced significantly. This result is in good agreement with the PZC studies, discussed earlier.

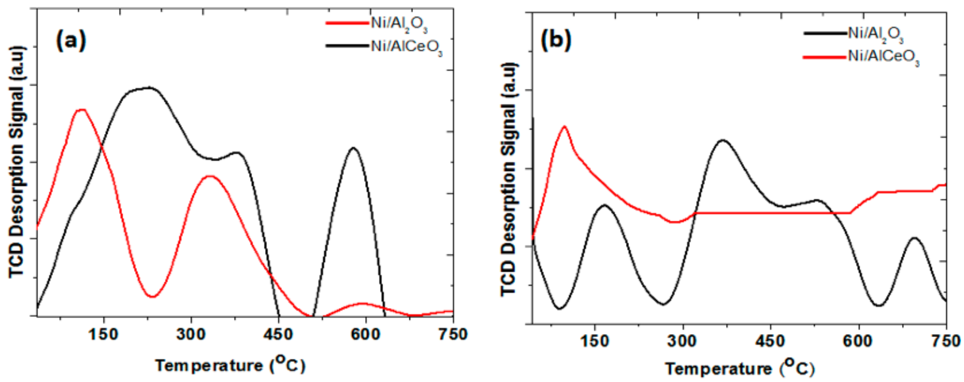

Figure 4. (**a**) CO_2–TPD and (**b**) NH_3–TPD profiles of the Ni/Al_2O_3 and $Ni/AlCeO_3$ catalysts.

Figure 4b presents the NH_3–TPD profiles obtained over the Ni/Al_2O_3 and $Ni/AlCeO_3$ catalysts. The Ni/Al_2O_3 presents a rather rich surface in terms of acid sites of weak, medium and high strength. Incorporation of Ce into the catalyst support leads to a drastic re-distribution of the acid sites of the catalyst, with only the weak sites dominating the surface. It is commonly accepted that on the surface of pure Al_2O_3 only the Lewis-type acid centres are observed. Miranda et al. [46] attributed desorption peaks at 77–277 °C and at 277–627 °C to the presence of two kinds of acid sites having different strengths. According to the authors, the lower desorption peak is linked to desorption of NH_3 bridge species which are bonded to penta-coordinated aluminum (Lewis weak sites), while the higher desorption peak to terminally bonded NH_3 on tri-coordinated aluminum (Lewis strong sites) [47]. Thus, it can be concluded that the high temperature acid sites correspond to the Brønsted acid sites of the solid surface [48] and the strong Lewis acid sites are associated with Al_2O_3 [47,49], whereas the low temperature acid sites are weak acid sites and mainly associated with CeO_2 [50] due to its generally weak basicity [39,51].

2.1.3. Ni species Reducibility

Metal-support interactions (electronic or geometrical) are crucial in defining the catalytic properties. In general, NiO interaction with the support, as well as the size of NiO, regulates the extent of its reduction. Weak interaction with the support is considered to give rise to reduction peaks at low temperatures, whereas peaks at high temperatures are due to a strong NiO-support interaction. In the H_2-TPR profile of the Ni/Al_2O_3 catalyst (Figure 5), two predominant peaks at 420 °C and 690 °C are apparent (Figure 5). The peak at 690 °C is due to the reduction of nickel aluminate ($NiAl_2O_4$), while the peak at 420 °C is due to small NiO crystallites interacting with the support (supported NiO). The small hump at 390 °C for the Ni/Al_2O_3 catalyst can be assigned to the reduction of bulk NiO [52]. The addition of Ce causes a redistribution of species and most likely changes the support size thus affecting the NiO-support contact area, with the latter being increased. This causes a reduction profile with peaks at lower temperatures compared with the Ni/Al_2O_3 catalyst.

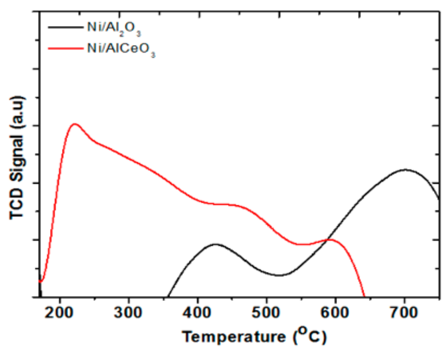

Figure 5. Temperature programmed reduction (TPR) profiles of Ni/Al_2O_3 and $Ni/AlCeO_3$ catalysts.

These TPR reduction profiles are in agreement with the ones presented by Yang et al. [53] where Ni/Al_2O_3 reduction takes place between 400–900 °C, whereas the addition of Ce gave rise to another reduction peak in the 200–400 °C region. This is due to the excellent redox properties of the Ce-related phases formed [54]. Thus, it can be concluded that the nickel species on the $AlCeO_3$ support retained a higher reducibility than Al_2O_3; the higher reducibility being a result of the incorporation of ceria into the alumina lattice [39]. Also, the complex profile of $NiO/AlCeO_3$ catalyst can be due to the fact that the nucleation and growth of the NiO over the Ce-modified Al_2O_3 is different compared to that of Al_2O_3. This could be due to the presence of new sites (e.g., Ce^{3+}, Al–O–Ce site, defects), which can act as anchoring sites for the growth of NiO, which affect the kinetics of the growth and ultimately the NiO size (distribution of NiO sizes). Furthermore, a support that exhibits strong metal-support interactions is anticipated to show less sintering during oxidation/reduction.

2.1.4. Surface Analysis

The XPS Ni 2p and Ce 3d peaks for both the calcined and reduced Ni/Al_2O_3 and $Ni/AlCeO_3$ catalysts are shown in Figure 6a–f. The Ni $2p_{3/2}$ peak for the calcined Ni/Al_2O_3 sample shows a peak at a binding energy of 856.1 eV, associated with the presence of $NiAl_2O_4$ (Figure 6a). The reduced catalyst also shows the presence of a main Ni $2p_{3/2}$ peak at a binding energy of 856.1 eV due to $NiAl_2O_4/Ni_2O_3$ but also a shoulder at lower binding energies at around 853 eV, due to the presence of metallic Ni (Figure 6b). For the $Ni/AlCeO_3$ catalysts, only the Ni $2p_{3/2}$ peak and satellite is shown in the Figure 6c,d as the $2p_{1/2}$ peak and satellite overlap with the Ce 3d peaks.

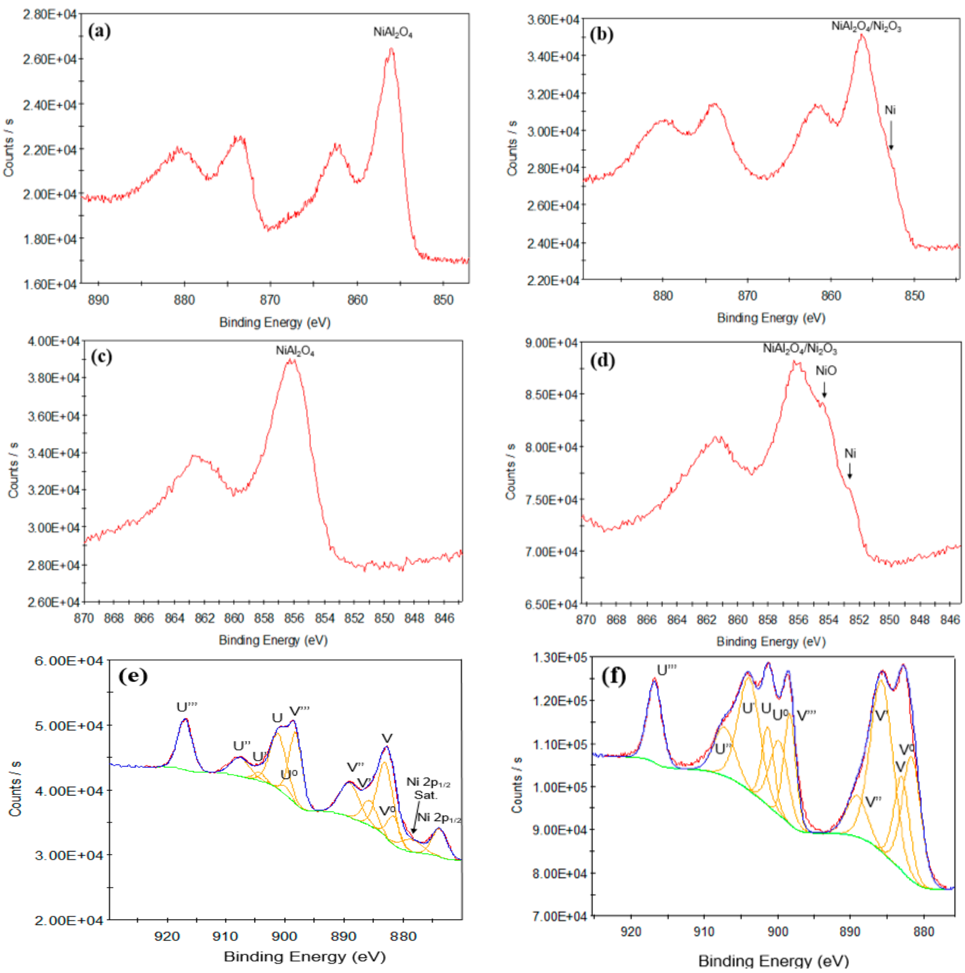

Figure 6. XPS Ni 2p for: (**a**) calcined Ni/Al_2O_3, (**b**) reduced Ni/Al_2O_3, (**c**) calcined $Ni/AlCeO_3$, (**d**) reduced $Ni/AlCeO_3$, and Ce 3d peaks for the calcined (**e**) and reduced (**f**) $Ni/AlCeO_3$ catalyst.

The calcined Ni/AlCeO_3 catalyst exhibits a Ni $2p_{3/2}$ peak at a binding energy of 856.2 eV due to $NiAl_2O_4$. The reduced Ni/AlCeO_3 catalyst shows a more complex peak shape with 3 components at binding energies of 856.2, 854.1 and around 852.6 eV. The complexity of the Ni 2p spectra in terms of their photoelectron and satellite features (particularly Ni oxide) precludes a sensible peak fit of the Ni 2p envelope [55]. The different components can be tentatively assigned to $NiAl_2O_4$/Ni_2O_3 (856.2 eV), NiO (854.1 eV) and Ni metal (852.6 eV). XPS Ce 3d photoelectron spectra for CeO_2 (Ce^{4+}) and Ce_2O_3 (Ce^{3+}) (Figure 6e,f) are also well known for their complex photoelectron and satellite peak structure [56–58]. Furthermore, for the catalyst surfaces examined here, overlap with the main Ni $2p_{1/2}$ satellite further complicates the spectral shape. Nevertheless, using standard spectra for CeO_2 and Ce_2O_3 recorded on this XPS instrument as a reference, and with the assistance of other XPS work on cerium oxides [56–58] the Ce 3d spectra have been peak fitted with a reasonable degree of certainty. The photoelectron and satellite peaks for the calcined Ni/AlCeO_3 catalyst are considered first (Figure 6e). The calcined catalyst surface shows peaks generally representative of Ce^{4+} (CeO_2). Using the nomenclature employed in previous XPS work on cerium oxide [56,57], the peaks are labelled v and u, corresponding to transitions associated with the Ce $3d_{5/2}$ and Ce $3d_{3/2}$ respectively. The peaks observed are those corresponding to the v, v″, v‴, u, u″ and u‴, corresponding to the Ce^{4+} species, hence CeO_2 is clearly the predominant oxide present. However, the peak fit shows the presence of weak peaks associated with the Ce^{3+} species (v_0, v′, u_0 and u′) and approximate fractions of the two oxide forms is 85% CeO_2 and 15% Ce_2O_3, corresponding to a stoichiometry of $CeO_{1.94}$. The peak shape agrees well with that given by Henderson et al., for a reported stoichiometry of $CeO_{1.95}$ [58]. For the reduced catalyst (Figure 6f), the Ce 3d spectrum is very different, with clear peaks present for both the Ce^{4+} (v, v‴, u, u″ and u‴) and Ce^{3+} (v′ and u′) species. The peak fit gives a ratio of 41% CeO_2 and 59% Ce_2O_3, corresponding to a stoichiometry of $CeO_{1.80}$. The peak shape recorded for the reduced Ni/AlCeO_3 catalyst agrees very well with the Ce 3d peak shapes shown for samples with reported stoichiometries of $CeO_{1.78}$ [56] and $CeO_{1.82}$ [58], having relative peak intensities in-between those observed for $CeO_{1.78}$ and $CeO_{1.82}$, as would be expected for a stoichiometry of $CeO_{1.80}$.

As is widely accepted, CeO_2 increases the dispersion of the metallic phase [59] and this is also observed for the catalysts tested herein with the results shown in Table 2. It has also been suggested that a high dispersion causes a specific interaction between the nickel and ceria species, were the Ni particles close to CeO_2 activate the dissociation of H_2 and by spillover favour the reduction of the ceria surface [60].

Table 2. Ni2p XPS data of calcined and reduced Ni/Al_2O_3 and Ni/AlCeO_3 catalysts.

Catalyst	Calcined Samples		Reduced Samples	
	Peak (BE)	**Atomic (at. %)**	**Peak (BE)**	**Atomic (at. %)**
Ni/Al_2O_3	856.05	2.69	856.04	2.76
Ni/AlCeO_3	856.16	3.86	855.74	3.54

2.2. *Catalytic Performance*

2.2.1. Total Conversion and Conversion to Gaseous Products

Figure 7a presents the results obtained following the catalytic tests, performed under experimental protocol #1, in terms of glycerol total conversion (X_{C3H8O3}, %) and glycerol conversion to gaseous products ($X_{C3H8O3\ gaseous}$, %) in relation to reaction temperature. It is clear that a very high conversion of glycerol was achieved by both catalysts, but also for the AlCeO_3 support, over the whole temperature range (from ≈85 at 400 °C to > 95% at 750 °C). In contrast, the total conversion of glycerol was relatively low for the bare alumina support, ranging from approximately 70% at 400 °C to 80% at 750 °C. The high conversion values recorded are due not only to the reforming of glycerol but also to its thermal decomposition, which can take place simultaneously during the GSR process [61–63].

The endothermic nature of the GSR reaction can be clearly deduced from the conversion of glycerol to gaseous products, which increases sharply with increasing temperature (Figure 7a).

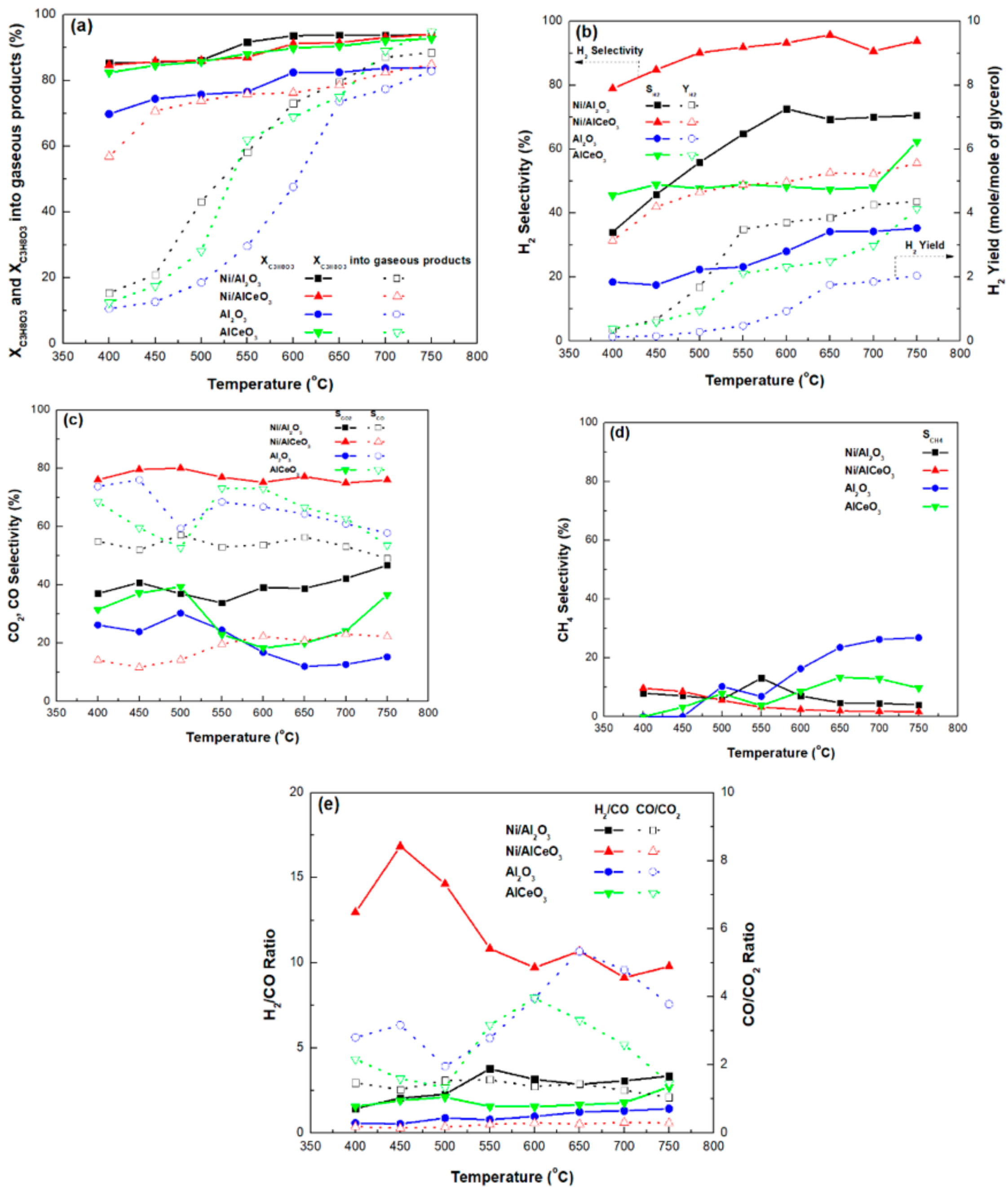

Figure 7. (**a**) Total glycerol conversion and glycerol conversion into gaseous products, (**b**) H_2 selectivity and H_2 yield, (**c**) CO_2 and CO selectivity, (**d**) CH_4 selectivity, and (**e**) H_2/CO and CO/CO_2 molar ratios (samples tested under experimental protocol #1).

However, it is clear that the Ni/AlCeO_3 catalyst produces a far greater number of gaseous products in comparison to Ni/Al_2O_3, especially for temperatures lower than 600 °C. Interestingly, the values of $X_{gaseous}$ for the Ni/AlCeO_3 sample ranged from 60% to 80% for the whole temperature range. Furthermore, the AlCeO_3 supporting material seems to produce more or less the same number of gaseous products as the Ni/Al_2O_3 catalytic sample. Previously published works [39] argued that the formation of CeAlO_3 perovskite structures suppresses any strong interaction between the nickel species and the Al_2O_3 support, thereby increasing the number of active sites and the reducibility of the active nickel species. From the results presented herein, the superior behaviour of the Ni/AlCeO_3 can be related to its higher dispersion (XPS), i.e., smaller Ni crystallites, and also to higher electron density and accessibility of the active sites caused by the close contact between nickel and the cerium species.

2.2.2. Gaseous Products' Selectivity

The influence of reaction temperature on H_2 selectivity (S_{H2}) and yield (Y_{H2}), following experimental protocol #1, for both catalysts and supports is presented in Figure 7b. As a first observation, the H_2 production of the Ni/AlCeO_3 catalyst is markedly higher in comparison to the Ni/Al_2O_3 sample for the whole temperature range, as its S_{H2} and Y_{H2} take the values of 80–90% and 4–6 mol/mol (6 mol/mol is very close to the value predicted by thermodynamics). This improved performance can also be observed for the AlCeO_3 support in comparison to the pure alumina. Thus, it can be suggested that the Ni active sites combined with the Brønsted acid sites promote the hydrogenolysis and dehydrogenation-dehydration of the bifunctional metal-acid Ni/AlCeO_3 catalyst, thereby converting more condensable intermediates into gaseous products, as well as leading to higher glycerol conversion and H_2 yield.

The influence of reaction temperature on the selectivity to CO_2 and CO (S_{CO2} and S_{CO}) for all samples is presented in Figure 7c. It is obvious that the Ni/AlCeO_3 sample is more selective towards CO_2 and less selective towards CO for the whole temperature range. This is in contrast to the trend observed for the Ni/Al_2O_3 catalyst and supporting materials, as these materials appear more selective towards CO and less selective towards CO_2. Thus, it seems that the ability to transform OHCs into H_2 and CO_2 is significantly higher for the Ni/AlCeO_3 catalyst probably due to its enhanced basic character (higher PZC value), which was introduced by the addition of CeO_2 to the alumina. Moreover, from Figure 7d it can be seen that both catalytic samples exhibit very low S_{CH4} for the whole temperature range; in contrast, S_{CH4} increases for the supports with increasing temperature. This was rather expected as according to the literature [36] at high water to glycerol feed ratios and at temperatures higher than 650 °C, the formation of CH_4 is strongly inhibited due to the methane steam reforming reaction being catalysed by the metallic active phase. Keeping in mind that glycerol decomposition to CH_4 during the reforming process is highly favoured [64], it appears that both catalysts have the capacity to reform the produced CH_4 into H_2 and CO.

Finally, the influence of reaction temperature on the H_2/CO and the CO/CO_2 molar ratios in the gaseous products' mixture is presented in Figure 7e. For the Ni/AlCeO_3 catalyst, the CO/CO_2 molar ratio is close to zero for the whole temperature range, while the H_2/CO molar ratio value decreases with increasing temperature from a value of about 17 (450 °C) to a value of about 10 (550–750 °C). In contrast, for the Ni/Al_2O_3 catalyst, both ratios are equal to 2–3 and appear relatively stable over the whole temperature range under investigation. The H_2/CO molar ratio value is more or less negligible for the supporting materials, whereas the CO/CO_2 molar ratio values range from about 2 between 400 and 500 °C, increases from 500 to 600 °C and decreases again for 650 °C $<$ T $<$ 750 °C (its maximum value was ~5.5 for the Al and ~4 for the AlCeO_3 sample). It is known that in the reaction process, dehydrogenation of the adsorbed glycerol molecule first takes place on the metal surface of catalyst to give adsorbed intermediates for the cleavage of C–C or C–O bonds.

From the results presented above it is obvious that the presence of ceria in the alumina supporting material has an important effect on the conversion and the gaseous product distribution, mainly by increasing H_2 and CO_2 production to the detriment of CH_4 and CO formation. It is likely that for the Ni/AlCeO_3 catalyst there is a first reaction step that involves rapid C–C breaking and CO formation, which is then followed by the WGS reaction, enhancing H_2 and CO_2 production. Sad et al. [65] has argued that acidic supports (such as alumina) favour the production of oxygenates (such as acrolein, acetol, acetaldehyde and acetic acid) via dehydration and dehydrogenation reactions, and that H_2 production is favoured by the use of non-acidic supports. However, the GSR process is also influenced by pyrolysis phenomena, given that the glycerol molecule is not thermally stable, which means that the intermediates formed by glycerol cracking are reformed on the catalyst surface [66].

2.2.3. Liquid Products' Selectivity

In accordance with previous research (e.g., [10,12,31]), a variety of liquid products were identified for the GSR however, only the main ones, i.e., acetone, acrolein, acetaldehyde, acetic acid, allyl alcohol, and acetol were quantified. The influence of temperature on liquid product selectivity for the Ni/Al_2O_3 and Ni/AlCeO_3 catalysts and the corresponding supports is shown in Figure 8. For the Ni/AlCeO_3 catalyst and the AlCeO_3 support, production of liquid effluents ceases over 700 °C, 50 °C higher compared to the Ni/Al_2O_3 sample. In contrast, pure alumina produces liquid effluents even at temperatures as high as 750 °C. Another important observation is the differences in the liquid product distribution between modified and unmodified samples. Specifically, for the Ni/AlCeO_3 and AlCeO_3, allyl alcohol seems to be the main product (at least for high temperatures), with acetaldehyde and acetone the secondary products. On the other hand, acetone is the main product at the high temperature range for the Ni/Al_2O_3 sample and acetic acid and acetol for pure alumina.

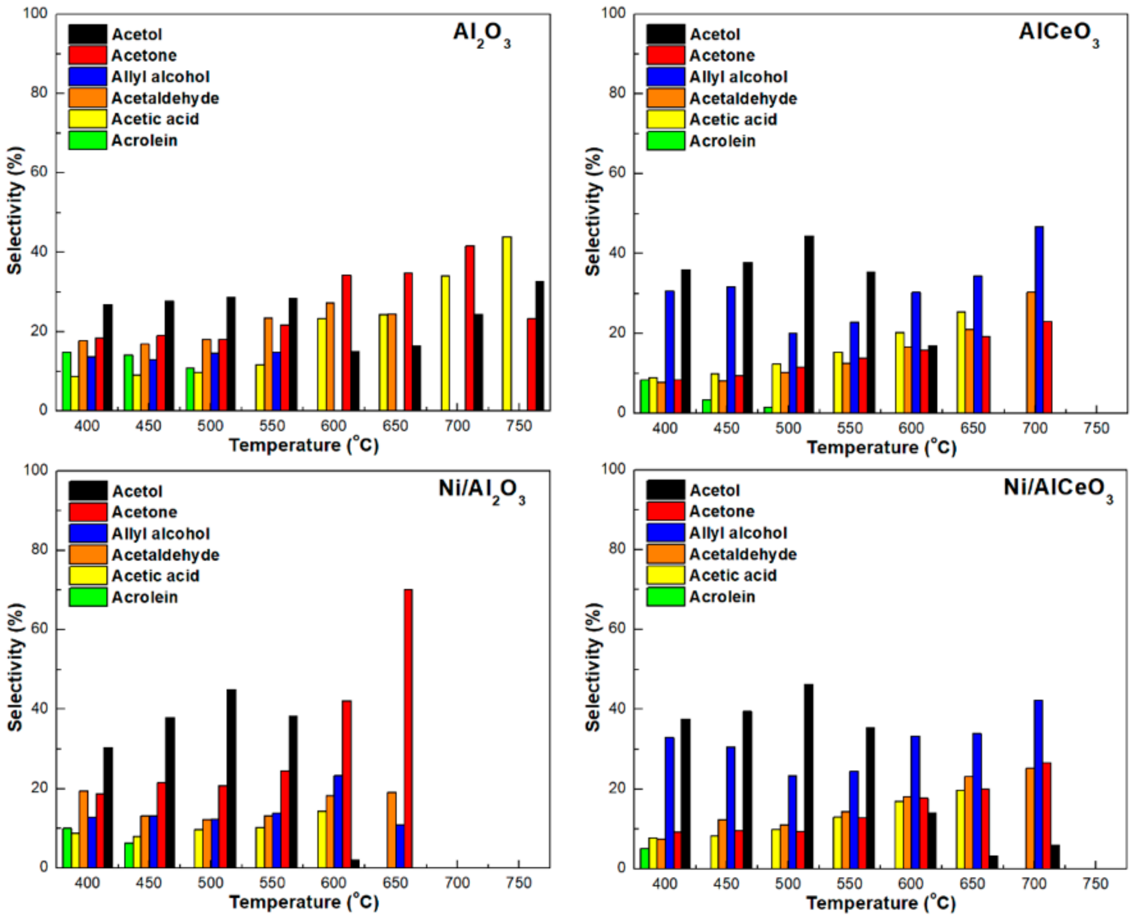

Figure 8. Liquid product selectivity for all samples tested herein (samples tested under experimental protocol #1).

According to the literature, there are four main reaction routes of glycerol consisting of three types of reactions, i.e., dehydrogenation, hydrogenolysis, and dehydration. These reactions represent the effects of the bifunctional metal–acid properties of the catalysts [47]. The first and the second routes of glycerol dehydrogenation and hydrogenolysis generate a common product, such as ethylene glycol, which is converted to acetaldehyde, glycolaldehyde, and ethanol. The hydrogenolysis of glycerol also produces methanol. The third route is glycerol dehydration to hydroxyacetone (acetol), which can be converted simultaneously in three ways to form a variety of products such as acetaldehyde, acetone, ethanol, acetic acid, propionic acid, formic acid, phenol, 1,2-propanediol, propanal, 1-propanol, and

2-cyclo-pentanone. This pathway is caused by the activation of the terminal OH of glycerol on the Lewis acid sites, which is represented by the strong acid sites of the catalysts. The fourth pathway is another glycerol dehydration reaction producing 3-hydroxypropanal, which is a starting reactant for the production of several chemicals. The species observed and confirming this pathway include allyl alcohol, acetaldehyde, methanol, formic acid, C_2H_4, and C_2H_6. This pathway involves the protonation of the secondary OH of glycerol to form acrolein, which favours the Brønsted acid sites mainly represented by the moderate acid sites [67].

2.3. Catalytic Stability

The results for catalytic stability are presented in Figure 9 and Table 3. It is noted that these experiments were carried out under more severe conditions (experimental protocol #2) in order to provoke carbon deposition and catalyst deactivation. From the results presented herein it is clear that although the Ni/AlCeO_3 catalyst suffers a slight decrease concerning glycerol total conversion (94–77%) and glycerol conversion to gaseous products (48–37%), it maintains remarkably stable values for H_2 yield (2.9–2.3) and selectivity (89–81%), as well as CO_2 (75–67%) and CO (23–29%) selectivity. As a result, the H_2/CO and CO/CO_2 molar ratios remain reasonably constant for the duration of the experiment, with values ranging between 9 to 6.5 and 0.3 to 0.4, respectively. The catalytic performance observed indicated that the effect of the WGS reaction do not weaken with time. It is accepted that the addition of basic modifiers, such as CeO_2 to Ni/Al_2O_3 catalysts can prevent carbon formation by favouring both the adsorption of H_2O, O_2, CO_2 or–OH fragments and the spillover of such fragments from the support to the metal particles [67], and thus facilitate carbon gasification.

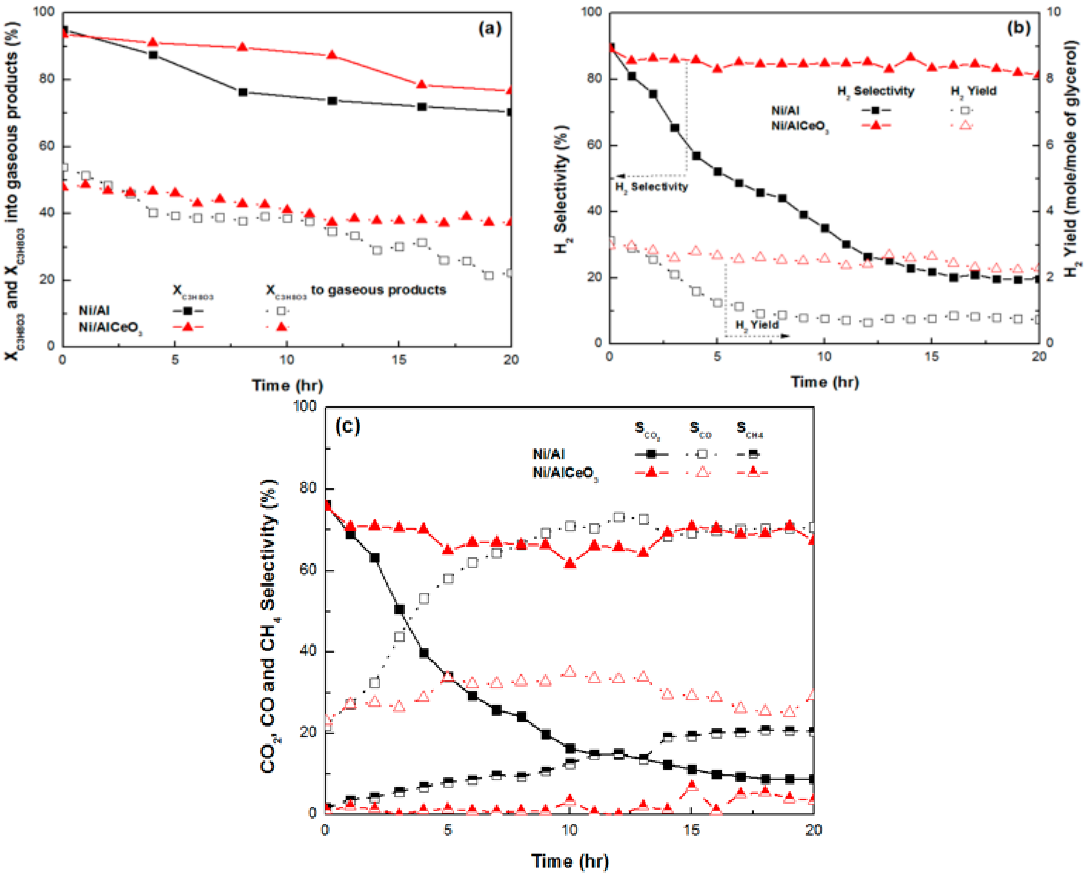

Figure 9. Time on stream experiments for Ni/Al_2O_3 and Ni/AlCeO_3 catalysts: (**a**) Total glycerol conversion and glycerol conversion into gaseous products, (**b**) H_2 selectivity and yield, (**c**) CO_2, CO and CH_4 selectivity (samples tested under experimental protocol #2).

Table 3. Catalytic performance of the Ni/Al_2O_3 and $Ni/AlCeO_3$ catalysts during time-on-stream at 600 °C (first and last measurement).

Reaction Metric	Ni/Al_2O_3		$Ni/AlCeO_3$	
	1st Measure	Last Measure	1st Measure	Last Measure
$X_{(C3H8O3)}$, %	95.03	70.42	93.58	76.69
$X_{(C3H8O3)}$, % into gaseous products	53.84	22.33	47.76	37.32
$Y_{(H2)}$, %	3.13	0.75	2.98	2.30
$S_{(H2)}$, %	89.85	19.74	89.19	81.47
$S_{(CO2)}$, %	76.17	8.78	75.72	67.26
$S_{(CO)}$, %	22.03	70.70	23.08	29.23
$S_{(CH4)}$, %	1.79	20.52	1.20	3.51
$S_{(acetol)}$, %	30.59	39.75	30.09	39.63
$S_{(acetone)}$, %	16.09	15.80	16.30	7.48
$S_{(allyl\ alcohol)}$, %	20.21	14.81	22.19	30.51
$S_{(acetaldehyde)}$, %	18.73	17.09	13.95	12.19
$S_{(acetic\ acid)}$, %	14.38	12.55	17.45	10.17
H_2/CO	9.51	0.65	9.02	6.51
CO/CO_2	0.29	8.06	0.31	0.44

In contrast, although the decrease in total X_{C3H8O3} and X_{C3H8O3} gaseous products for the Ni/Al_2O_3 catalyst was similar to the $Ni/AlCeO_3$, S_{H2}, Y_{H2} and S_{CO2} decreased substantially; this decrease was accompanied by an increase in the S_{CO} values. As a result, for the Ni/Al_2O_3 catalyst, the H_2/CO molar ratio decreased from 9.5 to 0.6 and the CO/CO_2 ratio increased from 0.3 to 8.0 with time on stream; a significant increase in methane production was also observed. The deactivation of Ni catalysts supported on pure alumina during the GSR reaction has also been reported by other research groups and has been attributed to carbon formation and sintering [68–70].

The difference in the catalytic behavior of the samples can be strongly affected by the nature of the carrier, suggesting that the activity and the rate of deactivation is likely to be related to the different extent of electronic interaction between supported metal and support, influencing the bonding and reactivity of the chemisorbed species. The presence of Ni^{2+}/Ni^0 and Ce^{4+}/Ce^{3+} couples means that different species can participate in the activation of the glycerol molecules. According to Bazin et al. [71] an increase of the local electron density is expected with increased metal dispersion, as has been proven for the $Ni/AlCeO_3$ catalyst; it exhibits a great number of active sites accessible to the reactant molecules compared to that observed for the Ni/Al_2O_3 catalyst.

2.4. Characterization of Used Catalysts

The nature of the carbonaceous deposits formed on to the spent catalytic samples following the time-on-stream experiments (experimental protocol #2) was examined using TPO, SEM, and TEM.

The TPO results for both catalysts are presented in Figure 10. As a first observation, significantly more carbon was deposited on to the Ni/Al_2O_3 catalyst (0.41 $g_{coke}/g_{catalyst}$) in comparison to the $Ni/AlCeO_3$ sample (0.14 $g_{coke}/g_{catalyst}$). The Ni/Al_2O_3 catalyst shows a weak peak at 470 °C and two broad peaks at 550 °C and 650 °C, which indicate the existence of different co-existing carbon allotropes. For the $Ni/AlCeO_3$ catalyst, there is a clear peak at ~375 °C, whereas a larger peak at 490 °C is observed; this points to the existence of coke that contains a higher fraction of defective carbon, which is known to be more easily oxidized. In addition, the high temperature decomposition peak appears as one single thermal event centred at 625 °C, i.e., slightly lower than the corresponding peak of the Ni/Al_2O_3 catalyst. It has been reported that the thermal decomposition of physisorbed carbonaceous products, termed as soft (or amorphous) coke, occurs at temperatures between 200 and 500 °C [39], while the gasification of hard coke (comprising of bulky carbonaceous species and often referred to as filamentous carbon) [72–74] takes place between 500 and 800 °C.

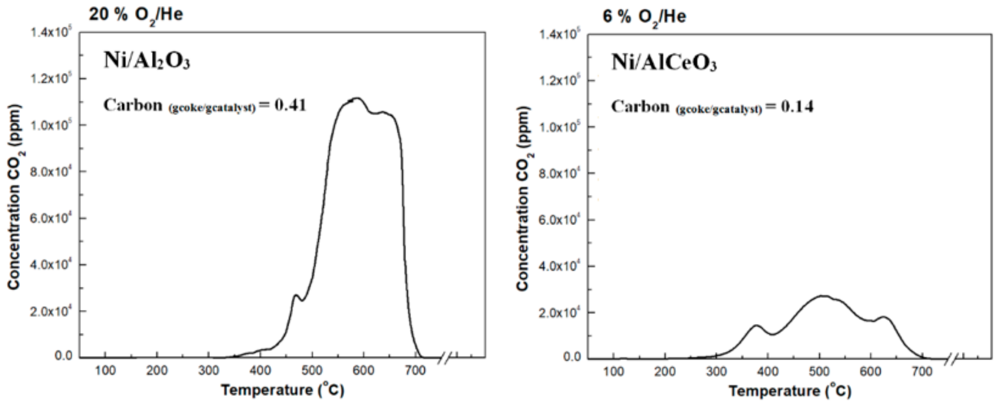

Figure 10. Temperature Programmed Oxidation (TPO) profiles and total amount of deposited carbon obtained for the spent Ni/Al_2O_3 and Ni/$AlCeO_3$ catalytic samples (samples tested under experimental protocol #2).

The hard coke species are 500–600 °C and can be associated with filamentous coke (carbon nanotubes, CNTs, and nanofibers, CNFs, that contain defects), whilst the coke gasified at over 600 °C can be associated with graphitic carbon species. This graphitic carbon is an inert coke that does not easily react with oxygen or steam [75]. Thus, not only was a higher quantity of coke deposited onto the spent Ni/Al_2O_3 catalyst, but also the fractions of graphitic carbon were greater and more difficult to oxidize than on the Ni/$AlCeO_3$ catalyst. These results explain the excellent stability observed for the Ni/$AlCeO_3$ catalyst. The different coke species on the catalyst surface can be formed by the Boudouard, methane decomposition and polymerization reactions [72,73]. Thus, the redox properties of CeO_2 and a higher dispersion of the active phase for the Ni/$AlCeO_3$ catalyst has resulted in markedly lower coke yields.

The morphology of the carbon deposits was initially examined using SEM/EDX; representative SEM micrographs and the carbon EDX images of the corresponding areas are shown in Figure 11. Although it is not straightforward to determine the precise nature of the coke deposits from this initial examination (i.e., whether these are nano-fibers, micro-fibers or carbon nanotubes), entangled tubular arrangements (filaments) can be discerned from the images. Also, the orientation of these filaments is quite random, which makes it difficult to estimate their length with any degree of accuracy. However, the EDX carbon images (red) show heavy coke deposition, particularly on the Ni/Al_2O_3 spent catalyst, in good agreement with the TPO results discussed above.

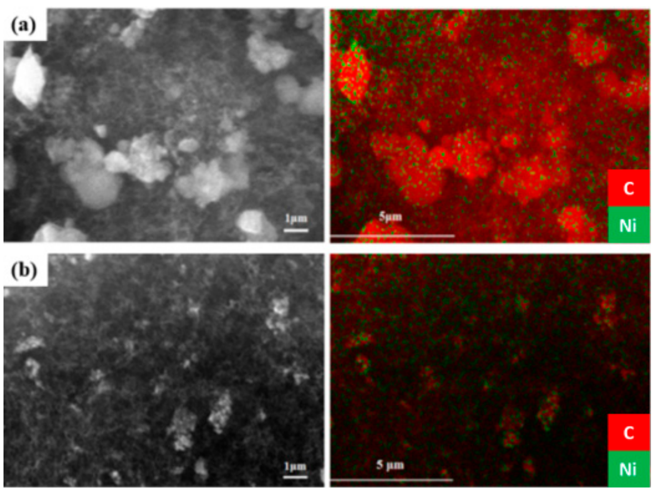

Figure 11. SEM images and carbon EDX images of the spent catalysts: (**a**) Ni/Al_2O_3, and (**b**) Ni/$AlCeO_3$ (samples tested under experimental protocol #2).

Figure 12 presents representative TEM images of the two spent catalytic samples and the corresponding particle size distribution histograms. The images confirm the formation of different carbon allotropes on the catalytic surface (indicated by black dashed circles), but also show heavy filament formation on the Ni/Al_2O_3 system, in excellent agreement with the discussion above. Encapsulating carbon can also be observed in the lower image for this system (examples of Ni particles are shown by red dashed circles), which is known to lead to a loss of activity as the Ni particle is no longer available during the reaction. Moreover, the particle size distribution histograms show that the mean Ni size of the Ni/$AlCeO_3$ catalyst is substantially smaller than that of the Ni/Al_2O_3, helping to explain the improved activity and stability characteristics of the former sample.

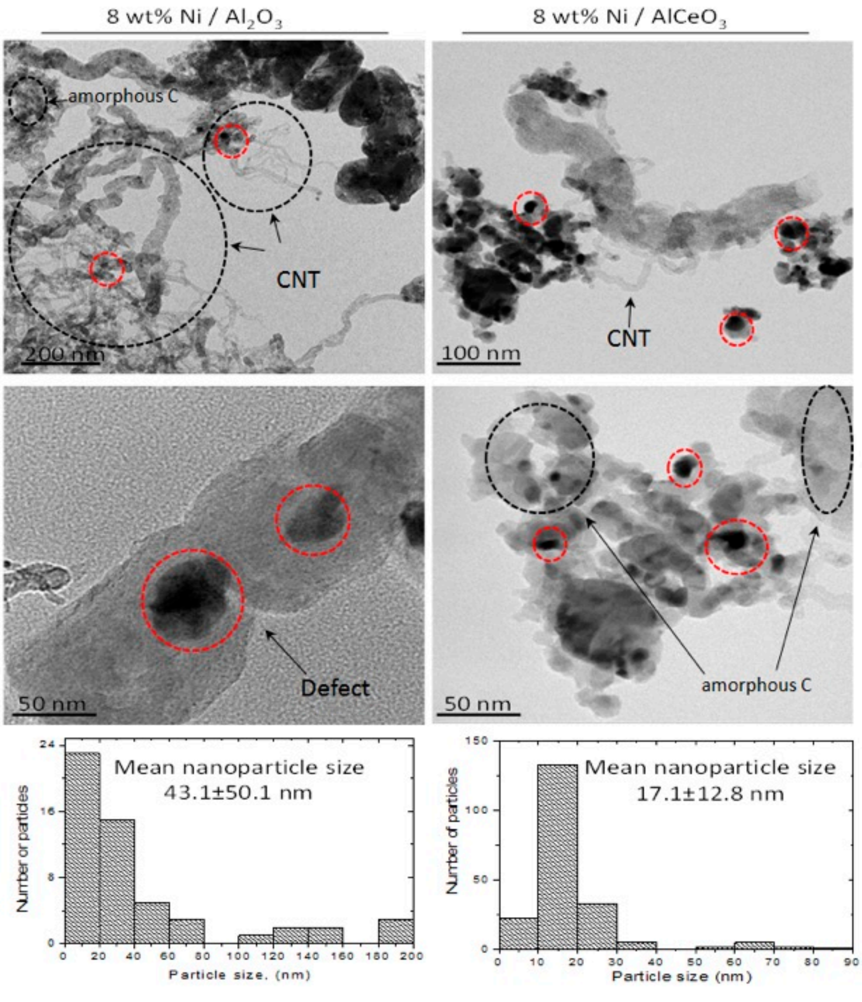

Figure 12. TEM images and particle size distribution of the Ni/Al_2O_3 and Ni/$AlCeO_3$ spent catalysts (samples tested under experimental protocol #2).

3. Materials and Methods

3.1. Catalyst Preparation

The alumina support (pellets) was acquired from Akzo, while the $AlCeO_3$ (powder) was sourced from Sigma Aldrich. The pelletized support was crushed and sieved to particle sizes in the range 350–500 μm, while the powder was first pelletized and then crushed to the same size. The catalysts were produced via the wet impregnation technique using an aqueous solution of $Ni(NO_3)_2$ $6H_2O$, obtained from Sigma Aldrich, with a concentration of 0.17 M to obtain catalysts with metal content of 8 wt %. The water contained in the slurries was evaporated under continuous stirring at 75 °C over

5 h. After, the suspensions were dried for 12 h at 120 °C and the calcination of the catalysts was carried out at 800 °C for 4 h.

3.2. Catalyst Characterization

For the determination of the catalysts' surface and bulk properties, different characterization techniques were employed. These included the calculation/determination of: (a) the Point of Zero Charge (PZC) for the calcined supports via Potentiometric Mass Titrations (PMTs), (b) the total specific surface area (SSA) of the catalytic materials and corresponding supports via the Brunauer–Emmet–Teller (BET) method, (c) the pore size distribution (PSD) of the catalytic materials and corresponding supports using the Barrett, Joyner, and Halenda (BJH) method, (d) the total metal loading (wt %) of the calcined catalysts using Inductively Coupled Plasma Atomic Emission Spectroscopy (ICP-AES), (e) the crystalline structure of the calcined supports, as well as the calcined and reduced catalysts by X-ray Diffraction (XRD) analysis, (f) the degree of Ni species reducibility using Temperature Programmed Reduction (H_2-TPR), (g) the acid and basic properties of the catalysts via CO_2- and NH_3-TPD experiments, (h) the nature of the various surface species and their oxidation states, on the reduced catalysts, using X-ray Photoelectron Spectroscopy (XPS) analysis, (i) the morphological characteristics of the spent catalysts using Scanning Electron Microscopy (SEM) and Transmission Electron Microscopy (TEM), and (j) the amount and nature of the carbonaceous deposits on the spent catalysts using Temperature Programmed Oxidation (TPO). The methodology and equipment used has been described in detail in previous publications by our group, and in particular: PZC in [26], XRD in [11], ICP at [76], and N_2 adsorption-desorption, H_2–TPR, CO_2–TPD, NH_3–TPD, XPS, SEM, TEM and TPO in [17,23].

3.3. Catalytic Tests

For the catalytic testing a continuous flow fixed-bed reactor was employed; the exact system and procedure has been described in detail in previous publications (e.g., [17,23]). Succinctly, using glycerol with 99.5% purity (Sigma-Aldrich, St. Louis, MO, USA) and a Weight Hourly Space Velocity (WHSV) of 50,000 mL g^{-1} h^{-1}, two different experimental protocols were employed. For the first protocol, the gas feed at the inlet of the reactor was a gas mixture of 73% H_2O, 4% $C_3H_8O_3$ and 23% He (i.e., 20 *v.v.* % of $C_3H_8O_3$ diluted in H_2O) and the catalytic performance was investigated between 400–750 °C. The second protocol was used for the investigation of catalytic stability during time-on-stream and was carried out for 20 h at 600 °C. The conditions chosen were more severe and the gas mixture at the reactor's inlet consisted of 63% H_2O, 7% $C_3H_8O_3$, 30% He (31° of $C_3H_8O_3$ diluted in H_2O). Before commencing the experiments, catalytic activation was undertaken in situ using a flow (100 mL min^{-1}) of high purity H_2 (5.0) at 800 °C for 1h. The system was then purged with He and the temperature lowered according to the protocol that was to be followed. The liquid products were analysed via a combination of Gas Chromatography (Agilent, Santa Clara, CA, USA, 7890A) and Mass Spectroscopy (Agilent 5975C). The gaseous products were determined via an Agilent gas chromatographer (7890A). Detailed information regarding the analysis of liquid and gaseous products can be found in Reference [11].

3.4. Reaction Metrics

The investigation of catalytic performance necessitated the calculation of total glycerol conversion, conversion of glycerol into gaseous products, and determination of the H_2 yield, H_2, CH_4, CO_2 and CO selectivity. For the calculations Equations (10) and (14) shown below were used. The selectivity of acetone [$(CH_3)_2CO$], acetaldehyde (C_2H_4O), acetol ($C_3H_6O_2$), allyl alcohol (CH_2=$CHCH_2OH$), acrolein (C_3H_4O) and acetic acid (C_2H_4O) was calculated based on Equation (15):

$$\%glycerol\ conversion_{(total\ conversion)} = \left(\frac{Glycerol_{in} - Glycerol_{out}}{Glycerol_{in}}\right) \times 100 \tag{10}$$

$$\%glycerol\ conversion_{(gaseous\ products)} = \left(\frac{C\ atoms\ in\ the\ gas\ products}{total\ C\ atoms\ in\ the\ feedstock}\right) \times 100 \quad (11)$$

$$H_2\ yield = \frac{H_2\ mol\ produced}{mol\ of\ glycerol\ in\ the\ feedstock} \quad (12)$$

$$\%H_2\ selectivity = \left(\frac{H_2\ mol\ produced}{C\ atoms\ produced\ in\ the\ gas\ phase}\right) \times \left(\frac{1}{RR}\right) \times 100 \quad (13)$$

where, RR is the reforming ratio (7/3), defined as the ratio of moles of H_2 to CO_2 formed.

$$\%\ selectivity\ of\ i = \left(\frac{C\ atoms\ in\ species\ i}{C\ atoms\ produced\ in\ the\ gas\ phase}\right) \times 100 \quad (14)$$

where, species *i* refers to CO, CO_2 and CH_4.

$$\%\ selectivity\ of\ i' = \left(\frac{C\ atoms\ in\ species\ i'}{C\ atoms\ produced\ in\ the\ liquid\ phase}\right) \times 100 \quad (15)$$

where, species i' refers to acetol, acetone, allyl alcohol, acetaldehyde, acrolein and acetic acid.

4. Conclusions

A critical assessment of the effect of the Ce-modification of Al_2O_3 on the catalytic performance of Ni/Al_2O_3 and Ni/$AlCeO_3$ catalysts towards glycerol steam reforming reaction and H_2 production has been performed. A thorough comparison of the $AlCeO_3$, Al_2O_3 (supports) as well as Ni/Al_2O_3 and Ni/$AlCeO_3$ (catalysts) has been presented.

The study has shown that Ce-modification of Al_2O_3 leads to a Ni catalyst with increased basicity (PZC and CO_2–TPD studies) and a higher Ni dispersion (H_2–TPR, XPS studies). The Ni/$AlCeO_3$ sample was more selective towards CO_2 and less selective towards CO. The opposite trend was observed for the Ni/Al_2O_3 catalyst. Importantly, both Ni/Al_2O_3 and Ni/$AlCeO_3$ had low CH_4 selectivity. For the Ni/$AlCeO_3$ catalyst the CO/CO_2 molar ratio was almost zero, while the H_2/CO molar ratio value decreases (from 17 to 10) with increasing temperature (450 °C to 750 °C). Regarding the liquid products for the Ni/$AlCeO_3$ and $AlCeO_3$, allyl alcohol was found to be the main product (at least for high temperatures), with acetaldehyde and acetone the secondary ones. On the other hand, acetone was the main product at the high T range for the Ni/Al_2O_3 sample and acetic acid and acetol for pure alumina. Stability studies performed for over than 20 h on stream showed that the Ni/$AlCeO_3$ catalyst experienced a slight decrease on glycerol total conversion (94–77%) and glycerol conversion to gaseous products (48–37%), but it maintained remarkably stable values for H_2 yield (2.9–2.3) and selectivity (89–81%), as well as for the CO_2 (75–67%) and CO (23–29%) selectivity. Characterization of the exhausted catalysts was performed in order to understand the nature of the deposited coke. It was found that Ni/$AlCeO_3$ was far more resistant to coke, while at the same time, it favored the formation of more defective carbon compared to the coke deposited onto Ni/Al_2O_3.

Author Contributions: Data curation, N.D.C., K.P. and M.A.G.; Formal analysis, N.D.C., B.D., V.S., S.J.H., M.A.B., K.P. and M.A.G.; Funding acquisition, K.P. and M.A.G.; Investigation, N.D.C. and G.I.S.; Methodology, N.D.C. and M.A.G.; Supervision, N.D.C., K.P. and M.A.G.; Writing—original draft, N.D.C., M.A.B., K.P. and M.A.G.; Writing—review & editing, N.D.C., M.A.B., K.P. and M.A.G.

Funding: This research received no external funding.

Acknowledgments: MAG: NDC and GIS are grateful for financial support by the program THALIS implemented within the framework of Education and Lifelong Learning Operational Programme, co-financed by the Hellenic Ministry of Education, Lifelong Learning and Religious Affairs and the European Social Fund, Project Title: "Production of Energy Carriers from Biomass by Products: Glycerol Reforming for the Production of Hydrogen, Hydrocarbons and Superior Alcohols". KP acknowledges the Abu Dhabi Department of Education and Knowledge (ADEK) through the Award for Research Excellence (AARE) 2017 and the Khalifa University through the RCII-2018-024 grant.

Conflicts of Interest: The authors declare no conflict of interest.

References

1. Hosseinzadeh-Bandbafha, H.; Tabatabaei, M.; Aghbashlo, M.; Khanali, M.; Demirbas, A. A comprehensive review on the environmental impacts of diesel/biodisel additives. *Energy Convers. Manag.* **2018**, *174*, 579–614. [CrossRef]
2. Boutesteijn, C.; Drabik, D.; Venus, T.J. The interaction between EU biofuel policy and first-and second-generation biodiesel production. *Ind. Crop. Prod.* **2017**, *106*, 124–129. [CrossRef]
3. Gebremariam, S.N.; Marchetti, J.M. Economics of biodiesel production: Review. *Energy Convers. Manag.* **2018**, *168*, 74–84. [CrossRef]
4. Charisiou, N.D.; Papageridis, K.N.; Siakavelas, G.; Tzounis, L.; Goula, M.A. Effect of active metal supported on SiO_2 for selective hydrogen production from the glycerol steam reforming reaction. *Bioresources* **2016**, *11*, 10173–10189. [CrossRef]
5. Weger, L.; Abanades, A.; Butler, T. Methane cracking as a bridge technology to the hydrogen economy. *Int. J. Hydrogen Energy* **2017**, *42*, 720–731. [CrossRef]
6. Callison, J.; Subramanian, N.D.; Rogers, S.M.; Chutia, A.; Gianolio, D.; Catlow, C.R.A.; Wells, P.P.; Dimitratos, N. Directed aqueous-phase reforming of glycerol through tailored platinum nanoparticles. *Appl. Catal. B Environ.* **2018**, *238*, 618–628. [CrossRef]
7. Jiang, B.; Li, L.; Bian, Z.; Li, Z.; Sun, Y.; Sun, Z.; Tang, D.; Kawi, S.; Dou, B.; Goula, M.A. Chemical looping glycerol reforming for hydrogen production by Ni@ZrO_2 nano-composite oxygen carriers. *Int. J. Hydrogen Energy* **2018**, *43*, 13200–13211. [CrossRef]
8. Polychronopoulou, K.; Charisiou, N.D.; Papageridis, K.N.; Sebastian, V.; Hinder, S.J.; Dabbawala, A.; AlKhoori, A.A.; Baker, M.A.; Goula, M.A. The effect of Ni addition onto a Cu-based ternary support on the H_2 production over glycerol steam reforming reaction. *Nanomaterials* **2018**, *8*, 931. [CrossRef]
9. Goula, M.A.; Charisiou, N.D.; Pandis, P.K.; Stathopoulos, V.N. Ni/apatite-type lanthanum silicate supported catalyst for the glycerol steam reforming reaction. *RSC Adv.* **2016**, *6*, 78954–78958. [CrossRef]
10. Bepari, S.; Pradhan, N.C.; Dalai, A.K. Selective production of hydrogen by steam reforming of glycerol over Ni/Fly ash catalyst. *Catal. Today* **2017**, *291*, 36–46. [CrossRef]
11. Goula, M.A.; Charisiou, N.D.; Papageridis, K.N.; Siakavelas, G. Influence of the synthesis method parameters used to prepare nickel-based catalysts on the catalytic performance for the glycerol steam reforming reaction. *Chin. J. Catal.* **2016**, *37*, 1949–1965. [CrossRef]
12. Papageridis, K.N.; Charisiou, N.D.; Siakavelas, G.; Avraam, D.G.; Tzounis, L.; Kousi, K.; Goula, M.A. Comparative study of Ni, Co, Cu supported on γ-alumina catalysts for hydrogen production via the glycerol steam reforming reaction. *Fuel Process. Technol.* **2016**, *152*, 156–175. [CrossRef]
13. Chen, H.; Ding, Y.; Cong, N.T.; Dou, B.; Dupont, V.; Ghadiri, M.; Williams, P.T. A comparative study on hydrogen production from steam-glycerol reforming: Thermodynamics and experimental. *Renew. Energy* **2011**, *36*, 779–788. [CrossRef]
14. Silva, J.M.; Soria, M.A.; Madeira, L.M. Challenges and strategies for optimization of glycerol steam reforming process. *Renew. Sustain. Energy Rev.* **2015**, *42*, 1187–1213. [CrossRef]
15. Charisiou, N.D.; Papageridis, K.N.; Siakavelas, G.; Tzounis, L.; Kousi, K.; Baker, M.A.; Hinder, S.J.; Sebastian, V.; Polychronopoulou, K.; Goula, M.A. Glycerol steam reforming for hydrogen production over nickel supported on alumina, zirconia and silica catalysts. *Top. Catal.* **2017**, *60*, 1226–1250. [CrossRef]
16. Dou, B.; Song, Y.; Wang, C.; Chen, H.; Xu, Y. Hydrogen production from catalytic steam reforming of biodiesel byproduct glycerol: Issues and challenges. *Renew. Sustain. Energy Rev.* **2014**, *30*, 950–960. [CrossRef]
17. Charisiou, N.D.; Siakavelas, G.; Papageridis, K.N.; Sebastian, V.; Hinder, S.J.; Baker, M.A.; Polychronopoulou, K.; Goula, M.A. The influence of SiO_2 doping on the Ni/ZrO_2 supported catalyst for hydrogen production through the glycerol steam reforming reaction. *Catal. Today* **2019**, *319*, 206–219. [CrossRef]
18. Aman, D.; Radwan, D.; Ebaid, M.; Mikhail, S.; van Steen, E. Comparing nickel and cobalt perovskites for steam reforming of glycerol. *Mol. Catal.* **2018**, *452*, 60–67. [CrossRef]
19. Charisiou, N.D.; Polychronopoulou, K.; Asif, A.; Goula, M.A. The potential of glycerol and phenol towards H_2 production using steam reforming reaction: A review. *Surf. Coat. Technol.* **2018**, *352*, 92–111. [CrossRef]

20. Senseni, A.Z.; Meshkani, F.; Rezaei, M. Steam reforming of glycerol on mesoporous nanocrystalline Ni/Al_2O_3 catalysts for H_2 production. *Int. J. Hydrogen Energy* **2016**, *41*, 20137–20146. [CrossRef]
21. Goula, M.A.; Charisiou, N.D.; Papageridis, K.N.; Delimitis, A.; Pachatouridou, E.; Iliopoulou, E.F. Nickel on alumina catalysts for the production of hydrogen rich mixtures via the biogas dry reforming reaction: Influence of the synthesis method. *Int. J. Hydrogen Energy* **2015**, *40*, 9183–9200. [CrossRef]
22. da Menezes, S.Q.J.P.; Manfro, R.L.; Souza, M.M.V.M. Hydrogen production from glycerol steam reforming over nickel catalysts supported on alumina and niobia: Deactivation process, effect of reaction conditions and kinetic modeling. *Int. J. Hydrogen Energy* **2018**, *43*, 15064–15082. [CrossRef]
23. Charisiou, N.D.; Papageridis, K.N.; Tzounis, L.; Sebastian, V.; Baker, M.A.; Hinder, S.J.; AlKetbi, M.; Polychronopoulou, K.; Goula, M.A. Ni supported on CaO-MgO-Al_2O_3 as a highly selective and stable catalyst for H_2 production via the glycerol steam reforming reaction. *Int. J. Hydrogen Energy* **2019**, *44*, 256–273. [CrossRef]
24. Chiodo, V.; Freni, S.; Galvagno, A.; Mondello, N.; Frusteri, F. Catalytic features of Rh and Ni supported catalysts in the steam reforming of glycerol to produce hydrogen. *Appl. Catal. A Gen.* **2010**, *381*, 1–7. [CrossRef]
25. Cheng, C.K.; Foo, S.Y.; Adesina, A.A. Steam reforming of glycerol over Ni/Al_2O_3 catalyst. *Catal. Today* **2011**, *178*, 25–33. [CrossRef]
26. Charisiou, N.D.; Siakavelas, G.; Papageridis, K.N.; Baklavaridis, A.; Tzounis, L.; Polychronopoulou, K.; Goula, M.A. Hydrogen production via the glycerol steam reforming reaction over nickel supported on alumina and lanthana-alumina catalysts. *Int. J. Hydrogen Energy* **2017**, *42*, 13039–13060. [CrossRef]
27. Yurdakul, M.; Ayas, N.; Bizkarra, K.; El Doukkali, M.; Cambra, J.F. Preparation of Ni-based catalysts to produce hydrogen from glycerol by steam reforming process. *Int. J. Hydrogen Energy* **2016**, *41*, 8084–8091. [CrossRef]
28. Zamzuri, N.H.; Mat, R.; Amin, N.A.S.; Talebian-Kiakalaieh, A. Hydrogen production from catalytic steam reforming of glycerol over various supported nickel catalysts. *Int. J. Hydrogen Energy* **2017**, *42*, 9087–9098. [CrossRef]
29. Charisiou, N.D.; Siakavelas, G.; Papageridis, K.N.; Baklavaridis, A.; Tzounis, L.; Avraam, D.G.; Goula, M.A. Syngas production via the biogas dry reforming reaction over nickel supported on modified with CeO_2 and/or La_2O_3 alumina catalysts. *J. Nat. Gas Sci. Eng.* **2016**, *31*, 164–183. [CrossRef]
30. Goula, M.A.; Charisiou, N.D.; Siakavelas, G.; Tzounis, L.; Tsiaoussis, I.; Panagiotopoulou, P.; Goula, G.; Yentekakis, I.V. Syngas production via the biogas dry reforming reaction over Ni supported on zirconia modified with CeO_2 or La_2O_3 catalysts. *Int. J. Hydrogen Energy* **2017**, *42*, 13724–13740. [CrossRef]
31. Demsash, H.D.; Mohan, R. Steam reforming of glycerol to hydrogen over ceria promoted nickel–alumina catalysts. *Int. J. Hydrogen Energy* **2016**, *41*, 22732–22742. [CrossRef]
32. Yentekakis, I.V.; Goula, G.; Panagiotopoulou, P.; Katsoni, A.; Diamadopoulos, E.; Matzavinos, D.; Delimitis, A. Dry reforming of methane: Catalytic performance and stability of Ir catalysts supported on γ-Al_2O_3, $Zr_{0.9}2Y_{0.08}O_{2-\delta}$ (YSZ) or $Ce_{0.9}Gd_{0.1}O_{2-\delta}$ (GDC) supports. *Top. Catal.* **2015**, *58*, 1228–1241. [CrossRef]
33. Yentekakis, I.V.; Goula, G.; Panagiotopoulou, P.; Kampouri, S.; Taylor, M.J.; Kyriakou, G.; Lambert, R.M. Stabilization of catalyst particles against sintering on oxide supports with high oxygen ion lability exemplified by Ir-catalyzed decomposition of N_2O. *Appl. Catal. B Environ.* **2016**, *192*, 357–364. [CrossRef]
34. Charisiou, N.D.; Siakavelas, G.; Tzounis, L.; Sebastian, V.; Monzon, A.; Baker, M.A.; Hinder, S.J.; Polychronopoulou, K.; Yentekakis, I.V.; Goula, M.A. An in depth investigation of deactivation through carbon formation during the biogas dry reforming reaction for Ni supported on modified with CeO_2 and La_2O_3 zirconia catalysts. *Int. J. Hydrogen Energy* **2018**, *43*, 18955–18976. [CrossRef]
35. Iriondo, A.; Barrio, V.L.; Cambra, J.F.; Arias, P.L.; Guemez, M.B.; Sanchez-Sanchez, M.C.; Navarro, R.M.; Fierro, J.L.G. Glycerol steam reforming over Ni catalysts supported on ceria and ceria-promoted alumina. *Int. J. Hydrogen Energy* **2010**, *35*, 11622–11633. [CrossRef]
36. Iriondo, A.; Barrio, V.L.; Cambra, J.F.; Arias, P.L.; Güemez, M.B.; Navarro, R.M.; Sanchez-Sanchez, M.C.; Fierro, J.L.G. Hydrogen production from glycerol over nickel catalysts supported on Al_2O_3 modified by Mg, Zr, Ce or La. *Top. Catal.* **2008**, *49*, 46–58. [CrossRef]
37. Buffoni, I.N.; Pompeo, F.; Santori, G.F.; Nichio, N.N. Nickel catalysts applied in steam reforming of glycerol for hydrogen production. *Catal. Commun.* **2009**, *10*, 1656–1660. [CrossRef]

38. Luisetto, I.; Tuti, S.; Battocchio, C.; Mastro, S.L.; Sodo, A. Ni/CeO_2-Al_2O_3 catalysts for the dry reforming of methane: The effect of $CeAlO_3$ content and nickel crystallite size on catalytic activity and coke resistance. *Appl. Catal. A Gen.* **2015**, *500*, 12–22. [CrossRef]
39. Kamonsuangkasem, K.; Therdthianwong, S.; Therdthianwong, A.; Thammajak, N. Remarkable activity and stability of Ni catalyst supported on CeO_2-Al_2O_3 via $CeAlO_3$ perovskite towards glycerol steam reforming for hydrogen production. *Appl. Catal. B Environ.* **2017**, *218*, 650–663. [CrossRef]
40. Bourikas, K.; Kordulis, C.; Lycourghiotis, A. Differential potentiometric titration: Development of a methodology for determining the point of zero charge of metal (hydro)oxides by one titration curve. *Environ. Sci. Technol.* **2005**, *11*, 4100–4108. [CrossRef]
41. Sing, K.S.W.; Everett, D.H.; Haull, R.A.W.; Moscou, L.; Pierotti, R.A.; Rouquerol, J.; Siemieniewska, T. Reporting physisorption data for gas/solid systems with special reference to the determination of surface area and porosity. *Pure Appl. Chem.* **1985**, *57*, 603–619. [CrossRef]
42. Rouquerol, F.; Rouquerol, J.; Sing, K. *Adsorption by Powders and Porous Solids*; Academic Press: Marseille, France, 1999.
43. Dou, B.; Wang, C.; Song, Y.; Chen, H.; Xu, Y. Activity of Ni–Cu–Al based catalyst for renewable hydrogen production from steam reforming of glycerol. *Energy Convers. Manag.* **2014**, *78*, 253–259. [CrossRef]
44. Charisiou, N.D.; Tzounis, L.; Sebastian, V.; Baker, M.A.; Hinder, S.J.; Polychronopoulou, K.; Goula, M.A. Investigating the correlation between deactivation and the carbon deposited on the surface of Ni/Al_2O_3 and Ni/La_2O_3-Al_2O_3 catalysts during the biogas reforming reaction. *Appl. Surf. Sci.* **2019**, *474*, 42–56. [CrossRef]
45. Aruna, S.T.; Kini, N.S.; Rajam, K.S. Solution combustion synthesis of CeO_2–$CeAlO_3$ nano-composites by mixture-of-fuels approach. *Matter. Res. Bull.* **2009**, *44*, 728–733. [CrossRef]
46. Miranda, B.C.; Chimentao, R.J.; Santos, J.B.O.; Gispert-Guirado, F.; Llorca, J.; Medina, F.; Bonillo, F.L.; Sueiras, J.E. Conversion of glycerol over 10%Ni/γ-Al_2O_3 catalyst. *Appl. Catal. B Environ.* **2014**, *147*, 464–480. [CrossRef]
47. Lif, J.; Odenbrand, I.; Skoglundh, M. Sintering of alumina-supported nickel particles under amination conditions: Support effects. *Appl. Catal. A Gen.* **2007**, *317*, 62–69. [CrossRef]
48. Guo, R.; Zhou, Y.; Pan, W.; Hong, J.; Zhen, W.; Jin, Q.; Ding, C.; Guo, S. Effect of preparation methods on the performance of CeO_2/Al_2O_3 catalysts for selective catalytic reduction of NO with NH_3. *J. Ind. Eng. Chem.* **2013**, *19*, 2022–2025. [CrossRef]
49. Shen, Y.; Zhu, S.; Qiu, T.; Shen, S. A novel catalyst of CeO_2/Al_2O_3 for selective catalytic reduction of NO by NH_3. *Catal. Commun.* **2009**, *11*, 20–23. [CrossRef]
50. Choudhary, V.R.; Rane, V.H. Acidity/basicity of rare-earth oxides and their catalytic activity in oxidative coupling of methane to C_2-hydrocarbons. *J. Catal.* **1991**, *130*, 411–422. [CrossRef]
51. Sato, S.; Takahashi, R.; Kobune, M.; Gotoh, H. Basic properties of rare earth oxides. *Appl. Catal. A Gen.* **2009**, *356*, 57–63. [CrossRef]
52. Li, G.; Hu, L.; Hill, J.M. Comparison of reducibility and stability of alumina-supported Ni catalysts prepared by impregnation and co-precipitation. *Appl. Catal. A Gen.* **2006**, *301*, 16–24. [CrossRef]
53. Yang, L.; Pastor-Perz, L.; Gu, S.; Sepulveda-Escribano, A.; Reina, T.R. Highly efficient Ni/CeO_2-Al_2O_3 catalysts for CO_2 upgrading via reverse water-gas shift: Effect of selected transition metal promoters. *Appl. Catal. B Environ.* **2018**, *232*, 464–471. [CrossRef]
54. Polychronopoulou, K.; Zedan, A.F.; Katsiotis, M.S.; Baker, M.A.; AlKhoori, A.A.; AlQaradawi, S.Y.; Hinder, S.J.; AlHassan, S. Rapid microwave assisted sol-gel synthesis of CeO_2 and $Ce_xSm_{1-x}O_2$ nanoparticle catalysts for CO oxidation. *Mol. Catal.* **2017**, *428*, 41–55. [CrossRef]
55. Grosvenor, A.P.; Biesinger, M.C.; Smart, R.S.C.; McIntyre, N.S. New interpretations of XPS spectra of nickel metal and oxides. *Surf. Sci.* **2006**, *600*, 1771–1779. [CrossRef]
56. Pfau, A.; Schierbaum, K.D. The electronic structure of stoichiometric and reduced CeO_2 surfaces: An XPS, UPS and HREELS study. *Surf. Sci.* **1994**, *321*, 71–80. [CrossRef]
57. Ardelean, H.; Frateur, I.; Marcus, P. Corrosion protection of magnesium alloys by cerium, zirconium and niobium-based coatings. *Corros. Sci.* **2008**, *50*, 1907–1918. [CrossRef]
58. Henderson, M.A.; Perkins, C.L.; Engelhard, M.H.; Thevuthasan, A.; Peden, C.H.F. Redox properties of water on the oxidized and reduced surfaces of CeO_2. *Surf. Sci.* **2003**, *526*, 1–18. [CrossRef]

59. Polychronopoulou, K.; Charisiou, N.D.; Siakavelas, G.I.; Alkhoori, A.A.; Sebastian, V.; Hinder, S.J.; Baker, M.A.; Goula, M.A. Ce-Sm-x Cu cost-efficient catalysts for H_2 production through the glycerol steam reforming reaction. *Sustain. Energy Fuels* **2019**, *3*, 673–691. [CrossRef]
60. Damyanova, S.; Pawelec, B.; Palcheva, R.; Karakirova, Y.; Capel Sanchez, M.C.; Tyuliev, G.; Gaigneaux, E.; Fierro, J.L.G. Structure and surface properties of ceria-modified Ni-based catalysts for hydrogen production. *Appl. Catal. B Environ.* **2018**, *225*, 340–353. [CrossRef]
61. Valliyappan, T.; Bakhshi, N.N.; Dalai, A.K. Pyrolysis of glycerol for the production of hydrogen or syngas. *Bioresour. Technol.* **2008**, *99*, 4476–4483. [CrossRef]
62. Wu, C.; Williams, P.T. Pyrolysis-gasification of post-consumer municipal solid plastic waste for hydrogen production. *Int. J. Hydrogen Energy* **2010**, *35*, 949–957. [CrossRef]
63. Bobadilla, L.F.; Penkova, A.; Romero-Sarria, F.; Centeno, M.A.; Odriozola, J.A. Influence of the acid-base properties over NiSn/MgO-Al_2O_3 catalysts in the hydrogen production from glycerol steam reforming. *Int. J. Hydrogen Energy* **2014**, *39*, 5704–5712. [CrossRef]
64. Li, Y.; Wang, W.; Chen, B.; Cao, Y. Thermodynamic analysis of hydrogen production via glycerol steam reforming with CO_2 adsorption. *Int. J. Hydrogen Energy* **2010**, *35*, 7768–7777. [CrossRef]
65. Sad, M.E.; Duarte, H.A.; Vignatti, C.; Padro, C.L.; Apesteguıa, C.L. Steam reforming of glycerol: Hydrogen production optimization. *Int. J. Hydrogen Energy* **2015**, *40*, 6097–6105. [CrossRef]
66. Chen, M.; Zhou, Z.; Wang, Y.; Liang, T.; Li, X.; Yang, Z.; Chen, M.; Wang, J. Effects of attapulgite-supported transition metals catalysts on glycerol steam reforming for hydrogen production. *Int. J. Hydrogen Energ.* **2018**, *43*, 20451–20464. [CrossRef]
67. Stosic, D.; Bennici, S.; Sirotin, S.; Calais, C.; Couturier, J.-L.; Doubois, J.-L.; Travert, A.; Auroux, A. Glycerol dehydration over calcium phosphate catalysts: Effect of acidic–basic features on catalytic performance. *Appl. Catal. A Gen.* **2012**, *447–448*, 124–134. [CrossRef]
68. Sanchez, E.A.; Comelli, R.A. Hydrogen production by glycerol steam-reforming over nickel and nickel-cobalt impregnated on alumina. *Int. J. Hydrogen Energy* **2014**, *39*, 8650–8655. [CrossRef]
69. Dieuzeide, M.L.; Jobbagy, M.; Amadeo, N. Glycerol steam reforming over Ni/γ-Al_2O_3 catalysts, modified with Mg (II). Effect of Mg (II) content. *Catal. Today* **2013**, *213*, 50–57. [CrossRef]
70. Iriondo, A.; Barrio, V.L.; El Doukkali, M.; Cambra, J.F.; Guemez, M.B.; Requies, J.; Arias, P.L.; Sachez-Sanchez, M.C.; Navarro, R.M.; Fiero, J.L.G. Biohydrogen production by gas phase reforming of glycerine and ethanol mixtures. *Int. J. Hydrogen Energy* **2012**, *37*, 2028–2036. [CrossRef]
71. Bazin, D.; Sayers, D.; Rehr, J.J.; Matteri, C. Numerical Simulation of the Platinum LIII Edge White Line Relative to Nanometer Scale Clusters. *J. Phys. Chem. B* **1997**, *101*, 5332–5336. [CrossRef]
72. Srisiriwat, N.; Therdthianwong, S.; Therdthianwong, A. Oxidative steam reforming of ethanol over Ni/Al_2O_3 catalysts promoted by CeO_2, ZrO_2 and CeO_2–ZrO_2. *Int. J. Hydrogen Energy* **2009**, *34*, 2224–2234. [CrossRef]
73. Zhang, H.; Shao, S.; Xiao, R.; Shen, D.; Zeng, J. Characterization of coke deposition in the catalytic fast pyrolysis of biomass derivates. *Energy Fuels* **2014**, *28*, 52–57. [CrossRef]
74. Sahoo, S.K.; Ray, S.S.; Singh, I.D. Structural characterization of coke on spent hydroprocessing catalysts used for processing of vacuum gas oils. *Appl. Catal. A Gen.* **2004**, *278*, 83–91. [CrossRef]
75. Koo, K.Y.; Lee, S.; Jung, U.H.; Roh, H.; Yoon, W.L. Syngas production via combined steam and carbon dioxide reforming of methane over Ni–Ce/$MgAl_2O_4$ catalysts with enhanced coke resistance. *Fuel Process. Technol.* **2014**, *119*, 151–157. [CrossRef]
76. Charisiou, N.D.; Baklavaridis, A.; Papadakis, V.G.; Goula, M.A. Synthesis gas production via the biogas reforming reaction over Ni/MgO-Al_2O_3 and Ni/CaO-Al_2O_3 catalysts. *Waste Biomass Valorization* **2016**, *7*, 725–736. [CrossRef]